PCCP

PAPER

View Article Online
View Journal | View Issue

Cite this: *Phys. Chem. Chem. Phys.*, 2020, **22**, 20303

Isomer-selected ion–molecule reactions of acetylene cations with propyne and allene†

P. C. Schmid, ‡[ab] J. Greenberg,‡[a] T. L. Nguyen, [c] J. H. Thorpe,[c] K. J. Catani,[a] O. A. Krohn, [a] M. I. Miller,[a] J. F. Stanton[c] and H. J. Lewandowski *[a]

Received 25th July 2020,
Accepted 30th August 2020

DOI: 10.1039/d0cp03953e

rsc.li/pccp

One of the fundamental goals of chemistry is to determine how molecular structure influences interactions and leads to different reaction products. Studies of isomer-selected and resolved chemical reactions can shed light directly on how form leads to function. In the following, we present the results of gas-phase reactions between acetylene cations ($C_2D_2^+$) with two different isomers of C_3H_4: propyne (DC_3D_3) and allene ($H_2C_3H_2$). Our highly controlled, trapped-ion environment allows for precise determination of reaction products and kinetics. From these results, we can infer details of the underlying reaction dynamics of $C_2H_2^+$ + C_3H_4. Through the synergy of experimental results and high-level quantum chemical potential energy surface calculations, we are able to identify distinct reaction mechanisms for the two isomers. We find long-range charge exchange with no complex formation is favored for allene, whereas charge exchange leads to an intermediate reaction complex for propyne and thus, different products. Therefore, this reaction displays a pronounced isomer-selective bi-molecular reactive process.

1 Introduction

Interactions between cold molecules and ions are thought to play a critical role in astrochemistry, in particular in the formation of complex molecules.[1] The study of such reactions thus has great promise for obtaining information relevant to the mechanisms that ultimately underlie the chemical diversity of the interstellar medium.[2] Additionally, the field of cold reactions provides a window through which one can explore hitherto unknown domains of chemistry and gain new insights into molecular processes. At low temperatures, interaction dynamics are sensitive to small details of the underlying potential energy surface. In this context, interesting chemistry has already been observed through ion–molecule reactions in cryogenic ion traps[3] and SIFT experiments.[4] While reactions between ions and nonpolar neutral diatomic molecules – mainly H_2 – are within the domain of Langevin dynamics, the characteristic temperature-independent behavior breaks down at cryogenic temperatures.[5] Further work in cryogenic systems has revealed subtle and novel effects in ion–molecule systems, such as reactive resonances, inverse kinetic temperature effects (counter to Langevin), and tunneling mediated reactions.[6]

More recently, the use of Coulomb crystals in ion gas-phase chemistry has produced significant results in probing the fundamental quantum behavior of charged atoms or molecules.[6–8] Coulomb crystals are formed when laser-cooled, trapped atomic cations, like Ca^+ or Yb^+, reach low enough temperatures to form ordered structures inside an ion trap potential.[9,10] Co-trapping molecular ions with the Coulomb crystal cools these ions to translational temperatures similar to the laser-cooled atomic ions.[11–13] This provides a low-temperature environment in which chemical reactivity (*via* ion–molecule reactions) can be probed in a detailed manner under controlled conditions, even down to the single ion level.[14] On the fundamental level, reactions between laser-cooled atomic ion and atoms,[15–18] as well as di- and tri-atomic molecules[19,20] have been studied. Coulomb crystals have enable detailed studies on the influence of internal states of a reactant, the effect of kinetic energy on a chemical reaction or even the influence of the molecular structure in reactions with atomic Ca^+.[21–25] Bi-molecular reactions of sympathetically cooled molecular ions have recently been studied in this unique environment.[26–29] The wealth of information on chemical reactions can be further increased when the ion trap is combined with a time-of-flight mass spectrometer (TOF-MS).[30–34] These systems offer the advantage of being able to determine

[a] *JILA and the Department of Physics, University of Colorado, Boulder, Colorado, USA. E-mail: lewandoh@jilau1.colorado.edu*
[b] *I. Physikalisches Institut, Universität zu Köln, Zülpicher Str. 77, 50937 Köln, Germany*
[c] *Quantum Theory Project, Departments of Chemistry and Physics, University of Florida, Gainesville, Florida, USA*

† Electronic supplementary information (ESI) available: Isomer-selected ion–molecule reactions of acetylene cations with propyne and allene. See DOI: 10.1039/d0cp03953e

‡ These authors contributed equally to this work.

absolute ion numbers,[33] which yields key information about branching ratios and rate constants in (complex) bi-molecular reactions. In recent studies, we used this experimental system to investigate the internal-state dependent reactions of laser-cooled Ca^+ ions with O_2[35] and NO,[36] as well as the bi-molecular reaction $CCl^+ + C_2H_2$.[37]

Here, we report on the investigation of the role of unsaturated compounds in bi-molecular reactions in organic chemistry, focusing on two fundamental systems: C_2H_2 and C_3H_4. Unsaturated hydrocarbons are key components in single-step reactions that lead to the growth of complex carbon chains in environments like the interstellar medium, extraterrestrial planetary atmospheres (*e.g.*, Titan), and soot formation. Acetylene has been observed in the interstellar medium (ISM)[38] and is a major contributor in the formation of complex molecules.[39–41] Also, the two isomers of C_3H_4, propyne ($HC{\equiv}C{-}CH_3$) and allene ($H_2C{=}C{=}CH_2$), are of relevance to the ISM and the chemical environment of Titan.[42] Additionally, the outcome of the reactions with either propyne or allene will increase the understanding about the influence of isomeric structure in ion-neutral bi-molecular reactions in organic chemistry.

We present an isomer-resolved study of the bi-molecular reaction between two organic molecules acetylene cation and isotope labelled C_3H_4 at translational temperatures below 120 K. Specifically, acetylene cations are sympathetically cooled with laser-cooled Ca^+ in a linear quadrupole radio-frequency (RF) trap and allowed to interact with two distinct isomers of C_3H_4: propyne and allene. Although both of these reactions take place on the same global potential energy surface, strikingly distinct results are obtained that reveal the underlying molecular complexity. We observe that both reactions produce $C_3H_3^+$ as a primary product, but only propyne has an additional primary reaction channel leading to the formation of $C_5H_5^+$. These outcomes are governed by a difference in the initial stage of the reaction of the two isomers. For reactions with allene, a direct, long-range charge exchange takes place, while propyne favors a short-range interaction leading to the formation of a intermediate reaction complex. From the combination of experimental results and quantum-chemical calculations, we are able to resolve the details of potential energy surfaces and can describe the dynamics of this reaction.

2 Methods

2.1 Experimental

We use a combined ion trap TOF-MS[33] for these experiments (Fig. 1). Reaction studies with, and characterization of, our linear Paul ion trap coupled to a TOF-MS have been described previously.[35–37] Here, we describe the details essential for studying reactions between $C_2D_2^+$ and C_3H_4. $C_2D_2^+$ cations are created *via* a 1 + 1 resonance enhanced multi-photon ionization scheme at 218 nm[43] produced from a nanosecond pulsed dye laser with 100 μJ per pulse. The laser is focused onto a supersonic beam of argon seeded with 6% C_2D_2 at the center of the ion trap to load acetylene cations. Then, neutral calcium

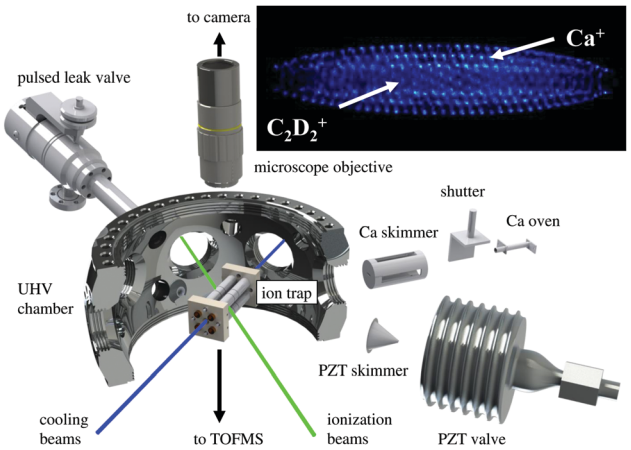

Fig. 1 Schematic render of the experimental apparatus. A cross-sectional view of the vacuum chamber reveals the ion trap at the center of our experiment. The skimmed, molecular beam enters the trap volume perpendicular to the trap axis. Ca^+ ions are produced by photoionization of an effusive source of calcium. For detection of the ions, either the fluorescence from the Ca^+ ions is collected by a microscope objective, or the ions are ejected into a TOF-MS, coupled radially to the ion trap. The microscope objective and pulsed leak valve are the only parts in the diagram outside of the vacuum chamber. The inset is a false-color fluorescence image of a typical bi-component Coulomb crystal of Ca^+ and $C_2D_2^+$ after loading and purification.

is non-resonantly photoionized inside the ion trap volume and co-trapped with $C_2D_2^+$. Laser cooling reduces the secular temperatures of Ca^+ to <1 K. The $C_2D_2^+$ molecules are sympathetically cooled *via* interactions with the Ca^+ until the ensemble crystallizes with a translational kinetic energy on the order of <1 K. RF secular excitation is used to eject unwanted contaminant ions from the Coulomb crystal,[44,45] thus creating a pure sample of $C_2D_2^+$ and Ca^+.

To initiate reactions, the neutral reactant, either propyne or allene (6% in Ar), is introduced into the vacuum chamber at constant pressure *via* a pulsed leak valve scheme.[35,46] The neutral gas increases the total pressure in the chamber to around 10^{-9} Torr, where the background pressure is around 10^{-10} Torr, as measured by a Bayard–Alpert hot-cathode ionization gauge. After an adjustable reaction time, the trap is turned off and high voltage is applied to the electrodes to extract all trapped ions into the TOF-MS. Using a calibrated TOF spectrum, we can determine the number of both reactant and product ions at each mass, and thus follow the reaction over time. The total number of ions is determined for every spectrum to assure the number of ions remains constant during a reaction and no product ions are lost from the system (see ESI† for more information).

An example image of a bi-component Coulomb crystal of $C_2D_2^+$ and Ca^+ before a reaction is shown as an inset in Fig. 1 (exemplary mass spectra corresponding to prior and after reaction are provided in the ESI†). For the results presented here, we used fully deuterated versions of acetylene (C_2D_2) and propyne (DC_3D_3), while in case of allene, $C_2D_2^+$ was reacted with fully hydrogenated allene ($H_2C_3H_2$). In both cases, the isotope tags were chosen to help elucidate reaction pathways and avoid product masses coinciding with Ca^+.

2.2 Theoretical

The potential energy surface of the reaction between propyne and acetylene cations, which proceeds *via* $C_5H_6^+$ intermediates, is calculated using a hybrid method referred to as CCSD(T)/ANO1//CCSD(T)/ANO0. The geometry optimization of the minima and transition states is performed using CCSD(T) in conjunction with the double-ζ, ANO0 basis. The electronic energy is then calculated at this geometry with CCSD(T) and the triple-ζ, ANO1 basis set. Harmonic zero-point corrections to the electronic energies are obtained with CCSD(T)/ANO0, and frequency analysis performed to confirm if the optimized structure corresponds to a minima or transition state. All quantum-chemical calculations are performed in the frozen-core approximation with the CFOUR package. It is expected that this method will yield relative energies accurate to within a few kcal mol^{-1}. RRKM rate calculations (including an asymmetric Eckart tunneling model) are then performed within the rigid-rotor harmonic-oscillator approximation, and unimolecular product branching ratios determined *via* the kinetic Master-Equation at 0 Torr.[47]

The potential energy surface of the reaction between allene and acetylene cations, which does not proceed through a $C_5H_6^+$ intermediate, involves species small enough to be treated with the mHEAT+ model chemistry. The details of mHEAT+ are discussed elsewhere.[48] This method should obtain relative energies to within 0.016 eV of experimental values. The frequencies of all stationary points are analysed to characterize them as minima or transition states.

3 Results

3.1 Acetylene and propyne

Three primary products are observed from the reaction $C_2D_2^+$ + DC_3D_3: $C_3D_3^+$, $C_3D_4^+$, and $C_5D_5^+$. Fig. 2 shows the measured ion numbers (normalized to the initial $C_2D_2^+$ ions) of reactants and products as a function of time. Secondary reaction products, $C_6D_5^+$ and $C_6D_7^+$, from the reaction $C_3D_4^+$ + DC_3D_3 are also observed, but have been omitted from the figure for clarity (see ESI† for details on secondary products). Neither $C_3D_3^+$ nor $C_5D_5^+$ products are observed to react further with neutral DC_3D_3. In Fig. 2, this is evident by a lack of ion depletion in the product channels at long reaction times. In contrast, $C_3D_4^+$ can be readily identified as an intermediate product, leading to mentioned higher-order reaction products. Due to the high detection sensitivity of our apparatus,[33] we can verify that no ions are lost from the trap over the course of a reaction (see ESI† for detailed information), and thus we can exclude the presence of additional, and unaccounted for, reactions.

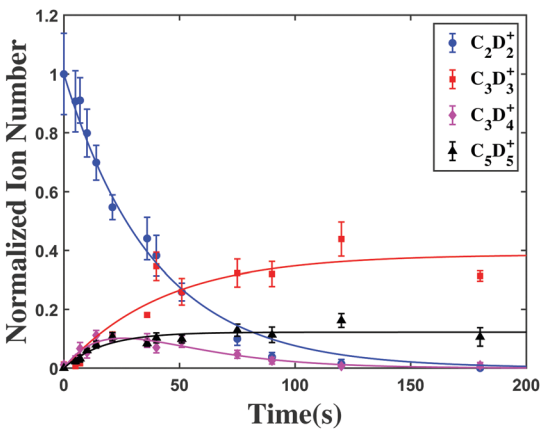

Fig. 2 Primary product formation from the reaction $C_2D_2^+$ + DC_3D_3 as a function of time. Each point represents the mean and standard error of seven measurements. The secondary reaction products $C_6D_5^+$ and $C_6D_7^+$ have been omitted for clarity (see ESI† for further details). Ion numbers are normalized to the initial number of $C_2D_2^+$ in the trap (typically ~150 ions). Reaction time corresponds to the amount of time the pulsed leak valve is open, and thus propyne is in the chamber.

The data are fit to extract reaction rates assuming pseudo first-order kinetics, where DC_3D_3 is in excess, using the following model:

$$\begin{aligned} C_2D_2^+ + DC_3D_3 &\rightarrow C_3D_3^+ + C_2D_3 \\ &\rightarrow C_3D_4^+ + C_2D_2 \\ &\rightarrow C_5D_5^+ + D \\ C_3D_4^+ + DC_3D_3 &\rightarrow \text{higher order products.} \end{aligned} \quad (1)$$

Reaction rate constants are determined by dividing out the concentration of the neutral reactant. This result is consistent with the Langevin model to within experimental accuracy and can be found in the ESI.†

3.2 Acetylene and allene

In contrast to the propyne results, $C_2D_2^+$ reacts with $H_2C_3H_2$ to produce mostly a single primary product, $C_3H_3^+$. $C_3H_3^+$ is not observed to react further with allene and continues to reside in the trap. Of the energetically allowed products, $C_5H_xD_y^+$ $(x+y=5)$ products are notably missing, which would be analogous to the product $C_5D_5^+$ in the propyne case. Fig. 3 shows the primary product channel as a function of time, as well as the depletion of reactant $C_2D_2^+$. Unlike in the propyne case, there is not enough accumulation of $C_3H_4^+$ in the trap to be able to directly measure this channel. A small quantity of heavier product carbocations ($C_6H_5^+$ and $C_6H_7^+$) are also detected. They are assumed to be the result from a secondary reaction between $C_3H_4^+$ and neutral $H_2C_3H_2$. It is important to note that all higher order products are the fully hydrogenated versions, with no deuterium from $C_2D_2^+$ incorporated. This indicates that there is no bond formed with $C_2D_2^+$ in the reaction process and points to a different reaction mechanism than in the case of $C_2D_2^+$ + DC_3D_3. Again, the data are fit to extract reaction rates assuming pseudo first-order kinetics, where allene is in excess, using the following model:

$$\begin{aligned} C_2D_2^+ + H_2C_3H_2 &\rightarrow C_3H_3^+ + C_2D_2 + H \\ &\rightarrow C_3H_4^+ + C_2D_2 \\ C_3H_4^+ + H_2C_3H_2 &\rightarrow \text{higher order products.} \end{aligned} \quad (2)$$

Identical to the propyne case, reaction rate constants were calculated by dividing out the neutral allene concentration.

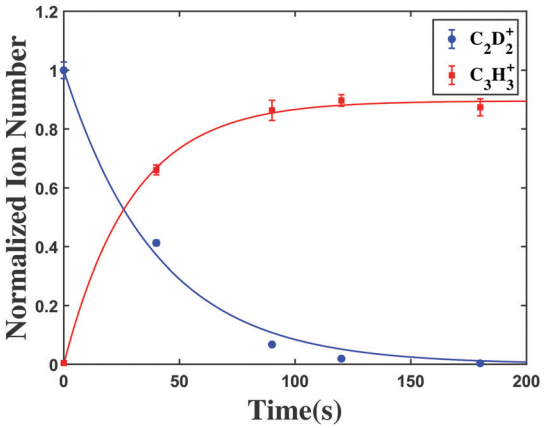

Fig. 3 Primary product formation from the reaction $C_2D_2^+ + H_2C_3H_2$ as a function of time. Each point represents the mean and standard error of 10 measurements. Higher-order products have been omitted for clarity. Ion numbers are normalized to the initial $C_2D_2^+$ in the trap, ~160 ions in these measurements. Reaction time corresponds to the amount of time the pulsed leak valve is open, and thus allene is in the chamber.

These results are also consistent with Langevin capture theory predictions, and can be found in the ESI.†

4 Discussion

4.1 Acetylene and propyne

The experimentally observed formation of the primary products $C_3D_3^+$ and $C_5D_5^+$ from the reaction of $C_2D_2^+$ with DC_3D_3 is indicative of a reaction pathway featuring a "long-lived", bound reaction complex between reactants. Fig. 4 displays a potential energy surface calculated with a CCSD(T)/ANO1//CCSD(T)/ANO0 scheme that comprises the salient stationary points (minima and transition states) for this system, where the (zero-point corrected) energies refer to the non-deuterated species. Given the considerable internal energy of the intermediate species on the PES, discrepancies between the deuterated and non-deuterated reaction kinetics is anticipated to be small.

The formation of the acetylene–propyne cation complex (culminating in complex INT0 in Fig. 4) is initiated by a charge transfer from $C_2H_2^+$ to HC_3H_3. This process is highly exothermic (by roughly 2 eV); the lack of collisional cooling in the Coulomb crystal, coupled with barrier heights below the entrance energy, enables the vibrationally hot complex to rapidly interconvert between the many minima displayed in Fig. 4. This reaction ultimately produces the observed primary reaction products $C_5H_5^+$, $C_3H_4^+$, and $C_3H_3^+$ *via* the loss of a hydrogen atom (PRD1, PRD3, and PRD5), the loss of an acetylene neutral (PRD4), and the loss of a vinyl radical (PRD2), respectively.

The product yields can be simulated by employing a chemical master equation model at the low-pressure (collisionless) limit, in conjunction with RRKM theory,[47] the details of which are described in the ESI.† We estimate that reactions between $C_2H_2^+$ and HC_3H_3, which proceed through the complex displayed in Fig. 4, result in product ratios of roughly 2 : 3 $C_3H_3^+$ to $C_5H_5^+$ (see ESI†), in contrast to the experimentally observed product ratios of 8 : 3 $C_3D_3^+$ to $C_5D_5^+$. We note that there is a maxima in the experimentally observed population of m/z 44 ($C_3D_4^+$, most likely $DC_3D_3^+$), at ~20 seconds. These ions go on to react with neutral DC_3D_3, leading to the depletion of signal of m/z 44. This suggests that another pathway may be in play, namely one where charge transfer between $C_2D_2^+$ and DC_3D_3 may occur, but formation of a reactive complex is suppressed. Combinations of long-range charge exchange mechanisms and short-range, bound, complex formation can be dependent on the reaction impact parameter. These effects have been studied in other ion–molecule systems, which investigated velocity map imaged (VMI) products from crossed-beam experiments.[49] Without a measured angle-dependent reactive cross-section, it is difficult to predict *a priori* the percentage of $DC_3D_3^+$ molecules that would take this second path. Bi-molecular reactions between $HC_3H_3^+$ and neutral HC_3H_3 have been studied previously,[50–52] and shown to produce a wide range of products, including $C_3H_3^+$ and $C_5H_5^+$, as well as higher order products $C_6H_5^+$ and $C_6H_7^+$.

In the current study, the form of the reaction curves for the primary products ($C_3D_3^+$ and – especially – $C_5D_5^+$) and the corresponding reaction rates show that these reactions are predominantly first order in the reactant. This is possible only by the formation of a reaction complex in the first reaction step of $C_2D_2^+ + DC_3D_3$, as shown in Fig. 4. The reaction $C_3D_4^+ + DC_3D_3$ is not observed to contribute to the primary product channels $C_3D_3^+$ or $C_5D_5^+$. This is consistent with previous studies of the reaction in the gas phase.[52]

4.2 Acetylene and allene

In contrast to DC_3D_3, only $C_3H_3^+$ is formed as a primary product (with appreciable yield) in the reaction between $C_2D_2^+$ and $H_2C_3H_2$. It is significant that only fully hydrogenated $C_3H_3^+$ is observed, as this suggests that no reaction complex between the two reactant species is formed. Otherwise, we would expect H/D exchange in the $C_3H_xD_y^+$ ($x + y = 3$) product channel and the reaction would enter the potential energy surface displayed in Fig. 4 at PRD4, which would invariably lead to some $C_5H_xD_y^+$ ($x + y = 5$) products.

The lack of reaction complex formation suggests that the reaction $C_2D_2^+ + H_2C_3H_2$ behaves differently than that with DC_3D_3. We propose that $C_2D_2^+$ and $H_2C_3H_2$ must undergo exclusively long-range charge transfer. A potential energy surface of the subsequent reaction of (undeuterated) $H_2C_3H_2^+$ cation is displayed in Fig. 5. It should be noted that this process (and the $C_2H_2^+$-allene surface in general) was first studied by Mebel and Bandrauk,[53] but was recalculated here with a higher level of theory (mHEAT+, see Methods section). If nearly all of the energy released in the charge-transfer process is transferred into $C_3H_4^+$ internal degrees of freedom, the $H_2C_3H_2$ cation first isomerizes to INT3 in Fig. 5, and then tunnels through TS3, passing through a post-reactive complex (PRC1) before fully dissociating a hydrogen and forming cyclic $C_3H_3^+$ (PRD1). These products are exothermic to the initial reactants by 0.016 eV (1.56 kJ mol^{-1}). $H_2C_3H_2^+$ is a Jahn–Teller system and

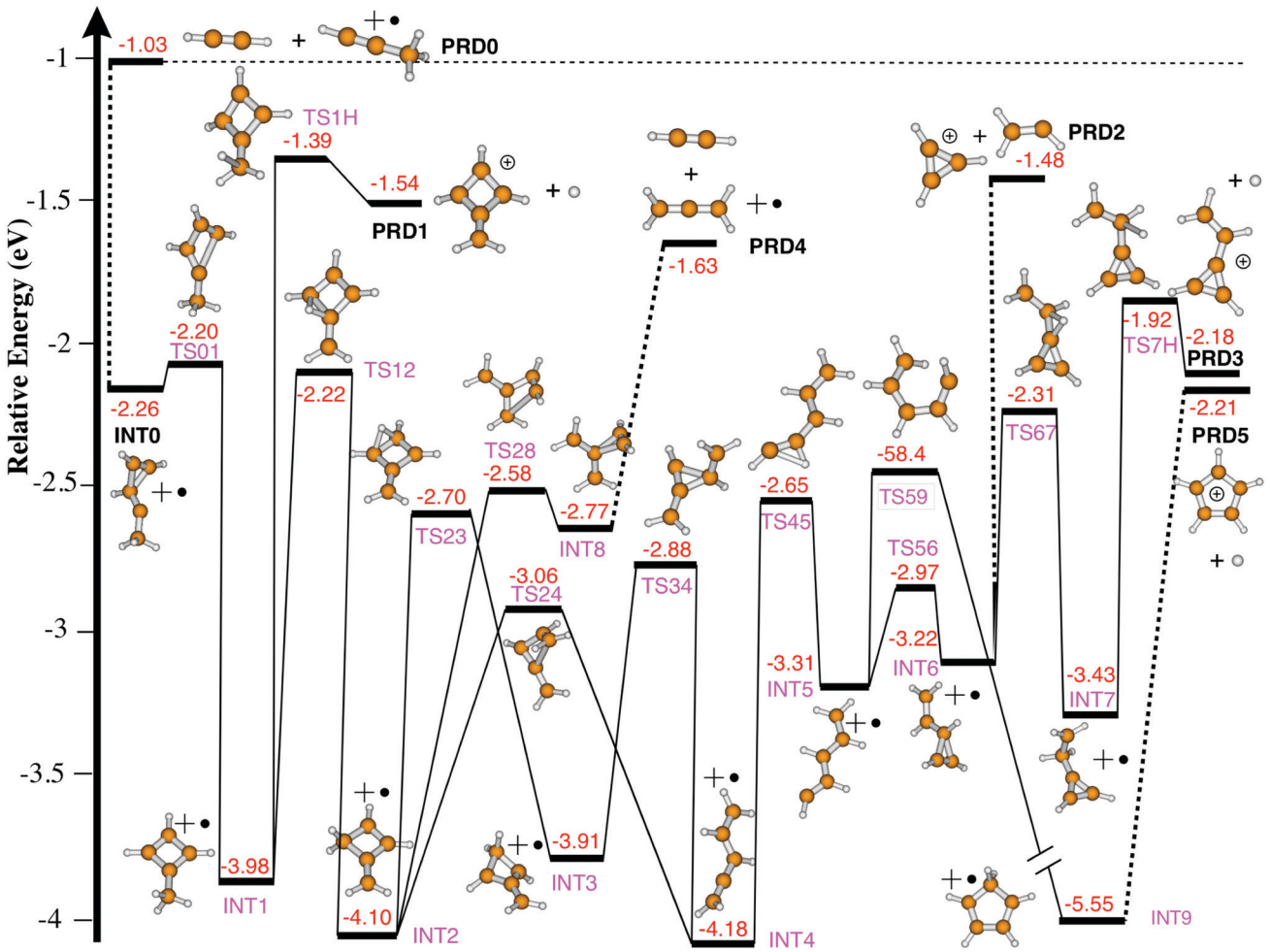

Fig. 4 Potential energy surface connecting the short-range charge transfer complex of acetylene cation and propyne to experimentally observed products. The energy of each stationary point is calculated using CCSD(T) in the scheme described in the text. All energies are relative to separated acetylene cation and propyne. Dashed lines between stationary points indicate reactions that occur *via* loose transition states. For the sake of clarity, PRD0 (top left) is already after the initial charge exchange between $C_2H_2^+$ + HC_3H_3.

distorts significantly from the geometry of the neutral, so this is a plausible explanation, since the distortion allows the energy from charge-transfer to populate the internal degrees of freedom necessary to undergo the isomerizations in Fig. 5. An analogous process has also been suggested in a VMI study of the charge transfer reaction C^+ + NH_3.[54] In this case, the authors observed evidence of a resonant energy transfer from the excess charge-exchange energy into the umbrella bending mode that connects the geometry of NH_3 to NH_3^+.

Almost all $H_2C_3H_2^+$ cations undergo the proposed mechanism leading to the very stable cyclic $C_3H_3^+$, save for a small population of $C_3H_4^+$ that goes on to react with $H_2C_3H_2$ neutrals to form larger products ($C_6H_5^+$ and $C_6H_7^+$). While it is somewhat surprising that all the internal energy available from direct charge transfer is converted to internal energy of the $H_2C_3H_2^+$ cation, our observations are consistent with the appearance potential of $C_3H_3^+$ observed in photoionization studies of $H_2C_3H_2$. These studies determined the appearance energy at just 1.79 eV above the threshold for ionization.[55] If the excess energy from the charge transfer is localized completely in $H_2C_3H_2^+$, it would be approximately 1.71 eV above this threshold, and the results observed here can be perhaps understood. In the photoionization experiments, samples of $H_2C_3H_2$ were ionized and detected much more quickly than the ions studied in this experiment, which allows more time for the H atoms to tunnel through the barrier. Thus, the tunneling process in the creation of c-$C_3H_3^+$ (TS3 in Fig. 5) is apparently quite efficient, and leads to a nearly 100% yield under the conditions of the Coulomb crystal experiment.

4.3 Isomer dependent pathways

The different proposed mechanisms for reactions between acetylene cations and propyne/allene, in the gas-phase, are driven by the different structure of the two isomers of C_3H_4. Here, we discuss the likely contributing factors that lead to a predominantly long-range, charge transfer interaction with allene, and a short-range, complex-forming interaction with propyne.

First, the acetylene cation charge transfer reaction with allene is overall more exothermic than that with propyne. The

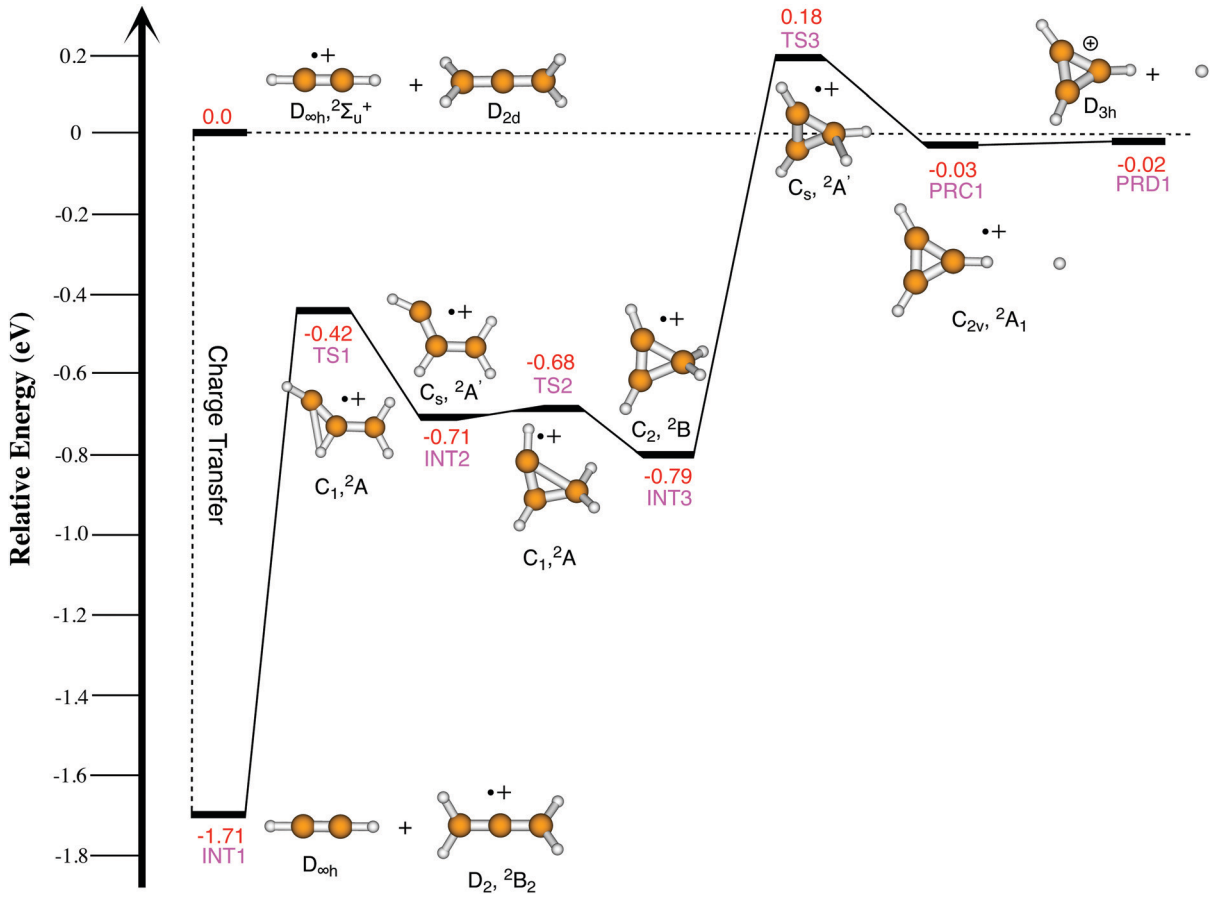

Fig. 5 Potential energy surface connecting d_0-allene and d_2-acetylene to the experimentally observed product. The energy of each stationary point is calculated using the mHEAT+ method. Note that the reaction proceeds *via* quantum tunneling through TS3 to form a nearly iso-energetic product.

generalized Mulliken–Hush treatment of electron transfer processes informs us that the reaction rate associated with long-range charge-transfer processes scales with the square of the overall reaction exothermicity.[56] Long-range in this context means the interaction potential between the molecules is weak (perturbative). Thus, long-range charge exchange will be kinetically preferred for allene as compared to propyne.

Second, because propyne has a (small) dipole moment, its Langevin capture radius will be larger than that of allene, which has no dipole moment. A larger radius of Langevin capture means that the formation of a close-range, bound complex will be kinetically more competitive to long-range charge transfer for propyne than it is with allene. Thus, the Langevin capture picture of the two reactions complements the Mulliken–Hush treatment.

Finally, there is a large difference in structure between neutral allene and its cation state, whereas there is almost no structural change between neutral propyne and its cation state. The relatively large distortion of allene upon ionization allows for almost all of the excess charge-transfer energy to be localized on the allene cation. The energy localization likely prevents the formation of a short-range, bound complex. This is in contrast to propyne where the charge-transfer energy is not localized by a Jahn–Teller distortion, and thus can be more easily shared across the resulting reaction complex.

These three considerations are all consistent with allene favoring a long-range charge transfer process, while propyne tends to form a reaction complex, as is observed in our experiment. In addition, a referee has shrewdly pointed out that the approach of C_3H_4 to $C_2D_2^+$ takes place on an excited state potential energy surface, which will interact—perhaps *via* a seam of conical intersections—with the ground state that comprises the charge-transferred $C_3H_4^+$ and C_2D_2 species. The nature of this interaction or conical interaction might very well play a role in the qualitatively different behavior for the propyne and allene isomers of C_3H_4 in the reaction with $C_2D_2^+$. Such an investigation provides a fourth possibility and is an appropriate topic for future study, but lies outside the scope of the present research.

It is due to the unique experimental environment provided by the Coulomb crystal – in particular the lack of internal cooling from collisions with a neutral background gas, which is common in typical ion cyclotron resonance (ICR) experiments – that the differences in product formation between these C_3H_4 isomers can be observed. The charge transfer is just exothermic enough to make unimolecular dissociation of $H_2C_3H_2^+$ possible, a process that likely would not occur in most other experiments since the hot ions would be subject to collisional cooling.

5 Conclusions

In conclusion, we have studied the isomer-specific reaction mechanism for the bi-molecular reaction between acetylene cations with two distinct isomers of C_3H_4, propyne and allene. For the reaction with propyne, we observed charge transfer and formation of a bound reaction complex that dissociated into two charged reaction products: $C_3D_3^+$ and $C_5D_5^+$. In contrast, the reaction with allene exhibited only long-range charge transfer followed by a tunneling mediated unimolecular decomposition. This reaction mechanism resulted in a single charged product: $C_3H_3^+$. The formation of a reaction complex in this system is hindered. High-level quantum chemical calculations were preformed to map out the potential energy surface for each reaction. Together with experimental results, we demonstrated that for this gas-phase reaction, the initial entry on to the PES is pivotal to the types of products formed. Thus, for the reaction between acetylene cations and propyne/allene, isomeric structure determines the outcome of the reaction.

In the future, reaction studies will be extended to probe the influence of the neutral reactants' quantum state and the collision energy on the reaction pathways. The additional control will be provided by using a travelling-wave Stark decelerator,[57,58] which will be coupled to the ion trap, similar to other work.[59,60] The Stark decelerator will allow a smooth variation of the speed of the neutral reactant down to 10 ms^{-1}, thus enabling reaction dynamics studies with sympathetically cooled molecular ions at temperatures as low as 10 K. Additionally, the molecules in the beam produced by a Stark decelerator can be in a single quantum state. These capabilities open up the possibility to study the influence of both external and internal degrees of freedom in ion–molecule reaction experiments.

Conflicts of interest

There are no conflicts to declare.

Acknowledgements

This work was supported by the National Science Foundation (PHY-1734006, CHE16-64325 and CHE-1900294), AFOSR (FA9550-16-1-0117), and NIST.

Notes and references

1 T. P. Snow and V. M. Bierbaum, *Annu. Rev. Anal. Chem.*, 2008, **1**, 229–259.
2 B. A. McGuire, *Astrophys. J., Suppl. Ser.*, 2018, **239**, 17.
3 D. Gerlich and M. Smith, *Phys. Scr.*, 2006, **73**, C25.
4 I. W. M. Smith and P. W. Barnes, *Annu. Rep. Prog. Chem., Sect. C: Phys. Chem.*, 2013, **109**, 140–166.
5 P. Tosi, O. Dmitriev, D. Bassi, O. Wick and D. Gerlich, *J. Chem. Phys.*, 1994, **100**, 4300–4307.
6 J. Toscano, H. J. Lewandowski and B. R. Heazlewood, *Phys. Chem. Chem. Phys.*, 2020, **22**, 9180–9194.
7 B. R. Heazlewood and T. P. Softley, *Annu. Rev. Phys. Chem.*, 2015, **66**, 475–495.
8 S. Willitsch, *Advances in Chemical Physics*, 2017, p. 307.
9 W. M. Itano and D. J. Wineland, *Phys. Rev. A*, 1982, **25**, 35–54.
10 M. Drewsen, *Phys. B*, 2015, **460**, 105–113.
11 T. Baba and I. Waki, *Jpn. J. Appl. Phys.*, 1996, **35**, L1134.
12 K. Mølhave and M. Drewsen, *Phys. Rev. A*, 2000, **62**, 011401.
13 A. Ostendorf, C. B. Zhang, M. A. Wilson, D. Offenberg, B. Roth and S. Schiller, *Phys. Rev. Lett.*, 2006, **97**, 243005.
14 A. K. Hansen, M. A. Sørensen, P. F. Staanum and M. Drewsen, *Angew. Chem., Int. Ed.*, 2012, **51**, 7960–7962.
15 F. H. J. Hall, M. Aymar, N. Bouloufa-Maafa, O. Dulieu and S. Willitsch, *Phys. Rev. Lett.*, 2011, **107**, 243202.
16 F. H. Hall, M. Aymar, M. Raoult, O. Dulieu and S. Willitsch, *Mol. Phys.*, 2013, **111**, 1683–1690.
17 L. Ratschbacher, C. Zipkes, C. Sias and M. Köhl, *Nat. Phys.*, 2012, **8**, 649.
18 R. Saito, S. Haze, M. Sasakawa, R. Nakai, M. Raoult, H. Da Silva, O. Dulieu and T. Mukaiyama, *Phys. Rev. A*, 2017, **95**, 032709.
19 N. Kimura, K. Okada, T. Takayanagi, M. Wada, S. Ohtani and H. A. Schuessler, *Phys. Rev. A*, 2011, **83**, 033422.
20 K. Okada, M. Wada, L. Boesten, T. Nakamura, I. Katayama and S. Ohtani, *J. Phys. B: At., Mol. Opt. Phys.*, 2003, **36**, 33.
21 S. Willitsch, M. T. Bell, A. D. Gingell, S. R. Procter and T. P. Softley, *Phys. Rev. Lett.*, 2008, **100**, 043203.
22 K. Okada, T. Suganuma, T. Furukawa, T. Takayanagi, M. Wada and H. A. Schuessler, *Phys. Rev. A*, 2013, **87**, 043427.
23 Y.-P. Chang, K. Długołecki, J. Küpper, D. Rösch, D. Wild and S. Willitsch, *Science*, 2013, **342**, 98–101.
24 P. Puri, M. Mills, I. Simbotin, J. A. Montgomery, R. Côté, C. Schneider, A. G. Suits and E. R. Hudson, *Nat. Chem.*, 2019, **11**, 615.
25 X. Tong, A. H. Winney and S. Willitsch, *Phys. Rev. Lett.*, 2010, **105**, 143001.
26 A. Kilaj, H. Gao, D. Rösch, U. Rivero, J. Küpper and S. Willitsch, *Nat. Commun.*, 2018, **9**, 2096.
27 L. Petralia, A. Tsikritea, J. Loreau, T. Softley and B. Heazlewood, *Nat. Commun.*, 2020, **11**, 1–7.
28 A. Kilaj, H. Gao, D. Rösch, U. Rivero, J. Küpper and S. Willitsch, *Nat. Commun.*, 2018, **9**, 1–7.
29 P. Puri, M. Mills, C. Schneider, I. Simbotin, J. A. Montgomery, R. Côté, A. G. Suits and E. R. Hudson, *Science*, 2017, **357**, 1370–1375.
30 P. Puri, S. J. Schowalter, S. Kotochigova, A. Petrov and E. R. Hudson, *J. Chem. Phys.*, 2014, **141**, 014309.
31 K. A. E. Meyer, L. L. Pollum, L. S. Petralia, A. Tauschinsky, C. J. Rennick, T. P. Softley and B. R. Heazlewood, *J. Phys. Chem. A*, 2015, **119**, 12449–12456.
32 D. Rösch, H. Gao, A. Kilaj and S. Willitsch, *EPJ Tech. Instrum.*, 2016, **3**, 5.
33 P. C. Schmid, J. Greenberg, M. I. Miller, K. Loeffler and H. J. Lewandowski, *Rev. Sci. Instrum.*, 2017, **88**, 123107.
34 S. Jyothi, K. N. Egodapitiya, B. Bondurant, Z. Jia, E. Pretzsch, P. Chiappina, G. Shu and K. R. Brown, *Rev. Sci. Instrum.*, 2019, **90**, 103201.

35 P. C. Schmid, M. I. Miller, J. Greenberg, T. L. Nguyen, J. F. Stanton and H. J. Lewandowski, *Mol. Phys.*, 2019, **117**, 3036–3042.
36 J. Greenberg, P. C. Schmid, M. Miller, J. F. Stanton and H. J. Lewandowski, *Phys. Rev. A*, 2018, **98**, 032702.
37 K. J. Catani, J. Greenberg, B. V. Saarel and H. J. Lewandowski, *J. Chem. Phys.*, 2020, **152**, 234310.
38 J. Lacy, N. J. Evans, J. Achtermann, D. Bruce, J. Arens and J. Carr, *Astrophys. J.*, 1989, **342**, L43–L46.
39 T. P. Snow and V. M. Bierbaum, *Annu. Rev. Anal. Chem.*, 2008, **1**, 229–259.
40 G. Floyd, R. Prince and W. Duley, *J. R. Astron. Soc. Can.*, 1973, **67**, 299.
41 J. Knight, C. Freeman, M. McEwan, V. Anicich and W. Huntress, *J. Phys. Chem.*, 1987, **91**, 3898–3902.
42 J. Waite, D. Young, T. Cravens, A. Coates, F. Crary, B. Magee and J. Westlake, *Science*, 2007, **316**, 870–875.
43 A. J. Orr-Ewing, R. A. Morgan, S. H. Wilson, C. L. Reed and M. N. Ashfold, *J. Chem. Soc., Faraday Trans.*, 1995, **91**, 3327–3337.
44 T. Baba and I. Waki, *J. Appl. Phys.*, 2002, **92**, 4109–4116.
45 B. Roth, P. Blythe and S. Schiller, *Phys. Rev. A: At., Mol., Opt. Phys.*, 2007, **75**, 023402.
46 C. Q. Jiao, D. R. A. Ranatunga, W. E. Vaughn and B. S. Freiser, *J. Am. Soc. Mass Spectrom.*, 1996, **7**, 118–122.
47 T. L. Nguyen and J. F. Stanton, *J. Phys. Chem. A*, 2015, **119**, 7627–7636.
48 J. H. Thorpe, C. A. Lopez, T. L. Nguyen, J. H. Baraban, D. H. Bross, B. Ruscic and J. F. Stanton, *J. Chem. Phys.*, 2019, **150**, 224102.
49 E. Carrascosa, J. Meyer and R. Wester, *Chem. Soc. Rev.*, 2017, **46**, 7498–7516.
50 J. J. Myher and A. G. Harrison, *J. Phys. Chem.*, 1968, **72**, 1905–1913.
51 M. T. Bowers, D. D. Elleman, R. M. O'Malley and K. R. Jennings, *J. Phys. Chem.*, 1970, **74**, 2583–2589.
52 C. Lifshitz, Y. Gleitman, S. Gefen, U. Shainok and I. Dotan, *Int. J. Mass Spectrom. Ion Phys.*, 1981, **40**, 1–16.
53 A. M. Mebel and A. D. Bandrauk, *J. Chem. Phys.*, 2008, **129**, 224311.
54 L. Pei and J. M. Farrar, *J. Chem. Phys.*, 2012, **136**, 204305.
55 J. Dannacher and J. Vogt, *Helv. Chim. Acta*, 1978, **61**, 361–372.
56 M. D. Newton and R. J. Cave, in *Molecular Electronics*, ed. M. A. Ratner, E. Jortner, J. Jortner and M. Ratner, 1996, p. 73.
57 M. Fabrikant, T. Li, N. Fitch, N. Farrow, J. D. Weinstein and H. Lewandowski, *Phys. Rev. A*, 2014, **90**, 033418.
58 Y. Shyur, J. A. Bossert and H. Lewandowski, *J. Phys. B: At., Mol. Opt. Phys.*, 2018, **51**, 165101.
59 J. M. Oldham, PhD thesis, University of Oxford, 2014.
60 P. Eberle, A. D. Dörfler, C. Von Planta, K. Ravi, D. Haas, D. Zhang, S. Y. van de Meerakker and S. Willitsch, *J. Phys.: Conf. Ser.*, 2015, 012012.

